Low Temperature Physics/Fizika Nizkikh Temperatur, 2014, v. 40, No. 10, pp. 1147–1154

Andreev-spectroscopy study of unconventional superconductivity in MgB_2:(La,Sr)MnO_3 nanocomposite

V.N. Krivoruchko, A.I. D'yachenko, and V.Yu. Tarenkov

Donetsk Institute for Physics and Engineering, National Academy of Sciences of Ukraine
72 R. Luxemburg Str., Donetsk 83114, Ukraine
E-mail: krivoruc@gmail.com

Received May 20, 2014, published online August 21, 2014

Unconventional high-temperature superconductivity in MgB_2:$La_{0:65}Sr_{0:35}MnO_3$ (MgB:LSMO) nanocomposite has been found recently [*Phys. Rev. B* **86**, 10502 (2012)]. In this report, the symmetry of the nanocomposite superconducting order parameter and plausible pairing mechanisms have been studied by the point-contact Andreev-reflection (PCAR) spectroscopy. To clarify the experimental results obtained, we consider a model of a ferromagnetic superconductor, which assumes a coexistence of itinerant ferromagnetism and mixed-parity superconductivity. The Balian–Werthamer state, with quasiparticle gap topology of the same form as that of the ordinary *s*-wave state, fits the experimental data reasonably well. Utilizing the extended Eliashberg formalizm, we calculated the contribution of MgB_2 in the total composite's conductivity and estimated the magnitude of the electron–phonon effects originated from MgB_2 in *I*–*V* characteristics of the composite at above-gap energies. It was found that distinctive features observed in the PC spectra of the MgB:LSMO samples and conventionally attributed to the electron–phonon interaction cannot be related to the MgB_2 phonons. It is argued that the detected singularities may be a manifestation of the electron-spectrum renormalizations due to strong magnetoelastic (magnon–phonon) interaction in LSMO.

PACS: **74.45.+c** Proximity effects; Andreev reflection; SN and SNS junctions;
74.78.–w Superconducting films and low-dimensional structures;
74.20.Rp BCS theory and its development;
74.81.–g Inhomogeneous superconductors and superconducting systems, including electronic inhomogeneities.

Keywords: unconventional superconductivity, heterostructures, Andreev reflection.

1. Introduction

Recently unconventional superconductivity in a binary network composed of *s*-wave superconductor MgB_2 and half-metallic ferromagnet $La_{0.65}Sr_{0.35}MnO_3$ was revealed [1]. Specifically, for MgB:LSMO (MgB_2:$La_{0.65}Sr_{0.35}MnO_3$) composites with 3:1 and 4:1 weight ratio (0.896:0.104 and 0.92:0.08 volume ratio, respectively) of components some principal effects have been found [1]. With an onset of the MgB_2 superconductivity, a spectacular drop of the sample resistance has been detected and superconductivity has been observed below 30 K. It was also found that the basic nanocomposites' characteristics (critical temperature, current–voltage dependence, percolation threshold, etc.) are strongly affected by the half-metallic (La,Sr)MnO_3 and cannot be quantitatively explained within the framework of the conventional percolation scenario. Using the point-contact (PC) spectroscopy, three energy gaps in the single-electron spectrum $\Delta_1(\pi)$, $\Delta_2(\sigma)$, and Δ_{tr} have been clearly revealed. Two of these gaps were identified as enhanced gaps in the quasiparticle spectrum of the MgB_2 in the composite. The third gap Δ_{tr} was about three times larger than the largest MgB_2 gap, and its magnitude is the same as those earlier detected in PCs data for (La,Ca)MnO_3 [2] and (La,Sr)MnO_3 [3] with Pb or MgB_2. A key feature is also the temperature behavior of the Δ_{tr} gap, which does not follow the BCS dependence.

As a possible explanation, it has been suggested [1–3] that doped manganites may be an example of systems with intrinsic fluctuated/incoherent superconductivity, i.e., with intrinsic $T_\Delta \neq 0$ but with global $T_\varphi = 0$ (here T_Δ stands for the temperature of an electron pairing, and T_φ is the temperature of a long-range phase coherency). That is, at low temperature in a half-metallic ferromagnet (La,Sr)MnO_3,

local spin-triplet *p*-wave pairing condensate already exists. However, though the local gap amplitude is large, there is no phase stiffness and the system is incapable of displaying a long-range superconducting response. Nonetheless, local phase rigidity survives and, being proximity coupled to MgB_2, the long-range coherency is restored. Inversely, the manganite in a superconducting state with large pairing energy enhances, due to proximity effect, the MgB_2 superconductivity.

To clarify the symmetry of the MgB:LSMO nanocomposite superconducting order parameter, we have examined a model which suggests that in the nanocomposite a superconducting phase develops in a low-symmetry environment with a missing inversion center. Namely, we consider a model of a ferromagnetic superconductor described by coexisting itinerant ferromagnetic and mixed-parity (a superposition of spin-singlet *s*- and spin-triplet *p*-waves) superconducting state. It is argued that a quasiparticle gap topology similar to that in the superfluid phase of ^{3}He [4] most probably is realized in the composite's superconducting phase.

In the BCS theory of superconductivity, electrons form (Cooper) pairs through an attractive interaction mediated by lattice vibrations. It is now generally accepted that the only mechanism of formation of Cooper pairs in MgB_2 is an electron–phonon interaction (EPI) [5,6]. Concerning ferromagnetic superconductors, Fay and Appel [7] predicted that longitudinal ferromagnetic fluctuations could result in a *p*-wave equal-spin-pairing superconducting state within the ferromagnetic phase.

As well established at present [8], the self-energy effects reveal themselves through the distinctive peculiarities in the PC current–voltage (*I–V*) dependence at $eV >> \Delta$. To elucidate a plausible pairing mechanism, which causes a superconducting pairing in the composite, we analyze experimental singularities observed in PCs spectra of the composite with nonmagnetic and ferromagnetic metallic wires. It was found that distinctive peculiarities observed in these PCs spectra and conventionally attributed to boson's self-energy effects cannot be related to the MgB_2 phonons. It is suggested that the detected singularities may be a manifestation of electron spectrum renormalizations due to a strong magnon–phonon (magnetoelastic) interaction in LSMO.

2. Specifics of experiment

The samples are composites of submicron MgB_2 powder and $La_{0.65}Sr_{0.35}MnO_3$ nanoparticles (about 20–30 nm in size). Details of the LSMO nanoparticles preparation were described earlier [9]. Comparative investigations of the nuclear magnetic resonance and nuclear spin-spin relaxation of ^{55}Mn nuclei of nanopowder and polycrystalline samples with the same composition confirmed the presence of the ferromagnetic metallic state and phase separation, which is typical for manganites, for particles of the size we used [10]. Powders with different weight ratios of LSMO and MgB_2 were mixed and cold pressed (under pressure up to 60 kbar) in stripes, and a number of samples of different composition was obtained.

The point contacts are made by direct touch of MgB:LSMO plate with sharpened needles of normal metals In, Ag, and Nb, and half-metallic ferromagnet (hmF) $La_{0.65}Ca_{0.35}MnO_3$ (LCMO). Since not every touch produces the desired appearance of the energy-gap *I–V* characteristics, we moved the electrodes relative to each other in order to penetrate through the accidentally damaged surface layer. This operation produces additional defects in the contact region and, thus, shortens further the small electron mean free path.

Small electron mean free path is one of a factor that hampers PC spectroscopy of manganites. However, as was earlier detected [6], even if the contact is obtained by the so-called "soft" point-contact technique, in which the larger (if compared to the electronic mean free path) "footprint" of the counter electrode is formed, these contacts very often provide spectroscopic information. This means that, on a microscopic scale, the real electrical contact occurs through parallel nanometric channels (whose number is unknown). The resistance of individual contacts is larger than the total contact resistance and usually is in the suitable range for Andreev reflection to occur. A selection of the "spectroscopic" contacts we made based on accordance of the PC's spectra to theoretical one for Andreev PC. The analysis of the PC spectra obtained (see Sec. 3.1) reveals the presence of small dips in the conductance. It was argued [11] that such dips are caused by the contact not being in the ballistic limit. We assume that our contact are in the diffusive regime [8].

A diffusive regime of electron current flow through a PC corresponds to significant *elastic* scattering of electrons in the PC area, with the *inelastic* electron scattering length l_{in} still exceeding the size of the contact *d*, i.e. $d/l_{in} << 1$. As is known [8], in the conventional case the contribution to the current through a constriction (*-c-*) between a superconductor (S) and a normal (N) metal (S-*c*-N contact) can be expressed, at $eV >> \Delta$, as a sum of four terms:

$$I(V) = V / R_N + I_N^{(1)}(eV) + I_{exc}^{(0)} + I_{exc}^{(1)}(eV) \ . \qquad (1)$$

Here R_N stands for the PC normal state resistance; $I_N^{(1)}$ is the negative increment to the current of the order of d/l_{in} as in the normal state because of EPI, i.e., due to an inelastic electronic relaxation mechanisms; $I_{exc}^{(0)}$ is the excess current [12] constant at $eV >> \Delta$. The term $I_{exc}^{(1)}$ is the energy-dependent correction to the excess current of the order of $I_{exc}^{(0)}(d/l_{in})$, which represents a contribution to the *I–V* curve proportional to Δ/eV for bias $eV >> \Delta$. Here elastic scattering due to a virtual emission and absorption of phonons causes the above-gap singularities. The elastic term is pro-

portional to the energy-dependent part of the excess current $I_{exc}(eV)$ and appears because of frequency dependence of the energy gap function $\Delta(\varepsilon = eV)$. At $T = 0$ the (normalized) difference conductance related to the excess current reads for the S-*c*-N contact [13–16]:

$$R_N \frac{dI_{exc}}{dV}(\varepsilon) = \left| \frac{\Delta(\varepsilon)}{\varepsilon + \sqrt{\varepsilon^2 - \Delta^2(\varepsilon)}} \right|^2, \quad \varepsilon = eV. \qquad (2)$$

Thus, similar to the tunneling spectroscopy, the self-energy effects can reveal themselves as the peculiarities already in the *first* derivatives of the PCs I_{exc}–V characteristic at large biases $eV >> \Delta$. Disappearance of peaks at rising temperature or magnetic field proves that they do not belong to the inelastic back scattering process, which should have the same intensity both in superconducting and in normal states [8]. Unfortunately, we are not able to destroy the superconductivity by magnetic field or by increasing temperature to distinguish directly elastic and inelastic electron scattering process contribution into PCs spectra. Nonetheless, we hope that some features observed in PC's dI_{exc}/dV characteristics provide evidence that the frequency dependence of the composite's energy gap $\Delta_{tr}(\varepsilon)$ differs from those for MgB_2. Note, that the differential conductance dI_{exc}/dV characteristics of any point contact (tunnel, ballistic, diffusive) are roughly similar in the region of $\varepsilon = eV$, where the contribution of $\mathrm{Im}\Delta(\varepsilon)$ is negligible (see, e.g., [16]). For MgB_2 this region is below 80 meV [5,6]. Just the energy range up to $eV \approx 80$ meV, where, for MgB_2, the self-energy structure is determined by $\mathrm{Re}\,\Delta(\varepsilon)$, will be under consideration below.

3. Results and discussion

3.1. Supercurrent spin polarization

Let us recall here that, at energies below the superconducting gap, a charge transport through a N metal being in contact with a S is possible only due to a specific process called Andreev reflection (AR) [17]. AR is a two-particle process in which, in the N metal, an incident electron above the Fermi energy ε_F and an electron below ε_F with opposite spins are coupled together and transferred across the interface in the S side forming a Cooper pair in the condensate. Simultaneously, a reflected hole with opposite momentum and spin appears in the N metal. The charge doubling at the interface enhances the subgap conductance and this phenomenon has indeed been observed in the case of a perfectly transparent interface. The picture is significantly modified when spin comes into play. If the N metal is a hmF there is full imbalance between spin-up and spin-down electron populations, which suppresses the AR and reduces the subgap conductance to zero. Particularly, LCMO is a hmF. Thus, if a supercurrent in the composite is unpolarized [*s*-wave or a *p*-wave ($S = 1$, $m = 0$) component of triplet pairing], in PCs of the composite with this hmF

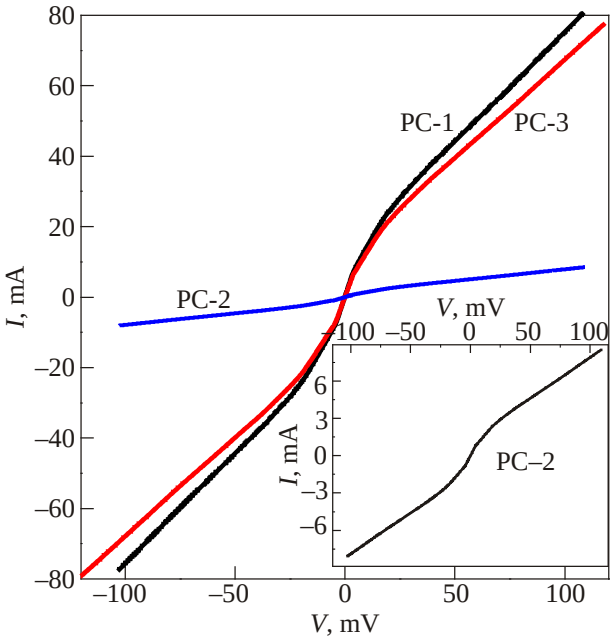

Fig. 1. (Color online) Current–voltage characteristics of three representative PCs $La_{0.65}Ca_{0.35}MnO_3$–composites (3:1); inset: the same for PC-2.

electrode the AR will be suppressed and the subgap conductance will be reduced below the normal-state value. On the contrary, if at both sides of the contact charge current is spin polarized, there is no restriction (because of spin) on the AR and, as in a conventional case, an excess current and a doubling of the normal-state conductance have to be observed.

In Figs. 1 and 2, we demonstrate typical PCs I–V dependences, Fig. 1, and the PC spectra, Fig. 2, of three re-

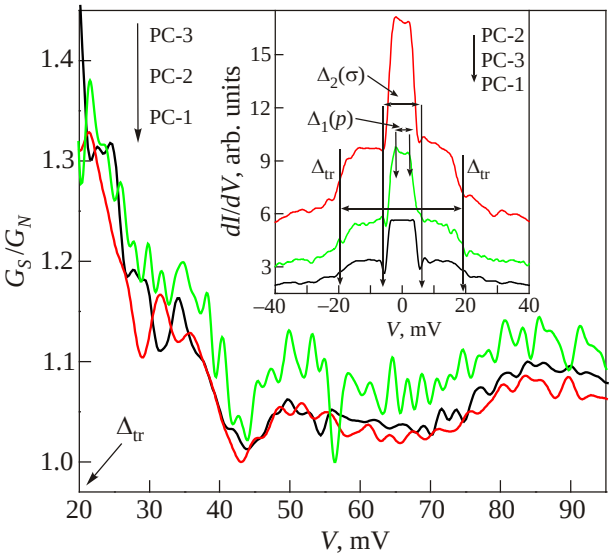

Fig. 2. (Color online) Normalized conductance $G_S/G_N = (dI/dV)_S/(dI/dV)_N$ of the PCs shown in Fig. 1 at $eV > \Delta_{tr}$. Inset: the AR spectra of these PCs; arrows point to the conductance drops corresponding to the superconducting gaps (the curves are shifted for convenience).

presentative contacts between the composite (3:1) and hmF electrode. As is seen in the figures, while the normal-state resistivity of the PCs differs by factor up to order, the contacts demonstrate common peculiarities (Fig. 1). Specifically, at low voltage, an excess current is unambiguously detected for all contacts. For all prepared contacts, we have observed almost doubling of the normal-state conductivity. In addition, at low voltage, dips in the differential conductance are clearly detected. Note that the PC differential conductance often shows sharp dips at voltage values larger that the superconducting gap, but as a rule very close to it. These dips are related to the superconducting properties of the S electrode since they never show up in N–N junctions, but the BTK theory is unable to reproduce them [6]. The different mechanisms leading to dips emergence are discussed in literature [11,18]. It has been shown that if dip is not too large (and a broadening parameter Γ introduced by Dynes *et al.* [19] is small) its position does not too much differ from the true energy gap magnitude. Within this approach, the single-electron energy gaps found are: $\Delta_1(\pi) \approx 1.9$–$2.3$ meV, $\Delta_2(\sigma) \approx 6.4$–$8.9$ meV, and $\Delta_{tr} \approx \approx 19.5$–$20.3$ meV. As already mentioned, two of these were identified as enhanced gaps originating from MgB_2. The third gap Δ_{tr} could not be related to *s*-wave superconductor MgB_2. The temperature dependence of the Δ_{tr} gap (see Fig. 8 in Ref. 1) does not follow the BCS dependence. These data are a strong argument in favor of a spin-polarized supercurrent in the MgB:LSMO composite. (A more detailed discussion one can find in Ref. 1.)

We also measured PCs characteristics between nonmagnetic In, Ag, and Nb tips and the composite (3:1). Figure 3 shows representative dynamic conductance spectra, $dI/dV = G(V)$, of such PCs. As in the case of a hmF needle (LCMO), at low voltage, doubling of the conductance and dips corresponding to three superconducting gaps with energies $\Delta_1(\pi)$, $\Delta_2(\sigma)$, and Δ_{tr} are observed, too.

The results shown in Figs. 1–3 are a noteworthy argument in favor of the mixed-parity superconducting state (a superposition of both spin-singlet and spin-triplet states) of the composite. Indeed, in the noncentrosymmetric superconductor both even-parity and odd-parity pairings are mixed, since no symmetry is available to distinguish between the two (see, e.g., [4,20]). Taking into account a nanoscale inhomogeneity of the composite, we suggest that the wave function of the composite superconducting state is also a superposition of both spin-singlet and spin-triplet contributions: $\Psi \sim a\Psi^s + b\Psi^{tr}$. The contributions from Ψ^s and Ψ^{tr} components are independent and, thus, the total supercurrent through the PC is

$$j \sim |\Psi|^2 = |a\Psi^s + b\Psi^{tr}|^2 = a'|\Psi^s|^2 + b'|\Psi^{tr}|^2 .$$

Generally, the relative weight of singlet and triplet components in a pair wave function depends on the ratio of the pairing interactions decomposed into even- and odd-

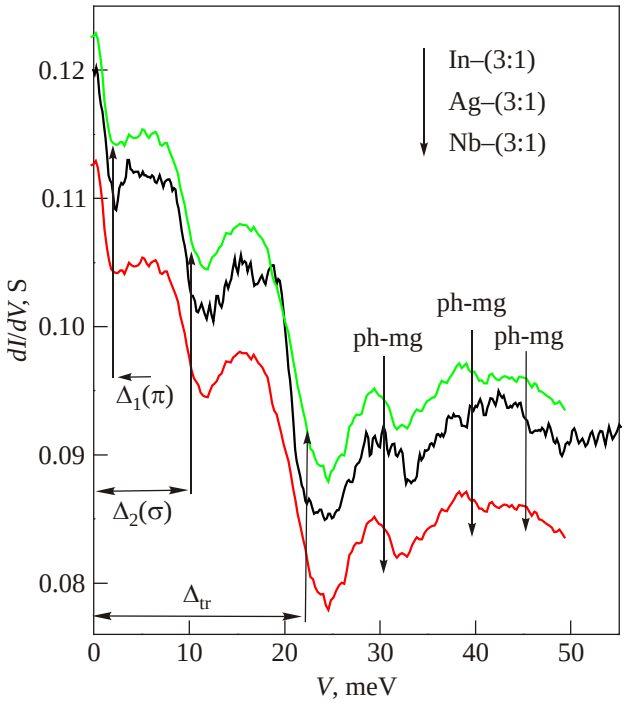

Fig. 3. Dynamic conductance spectra of the PCs between nonmagnetic In, Ag, and Nb tips and the composite (3:1). Arrows point to the conductance drops corresponding to the superconducting gaps $\Delta_1(\pi)$, $\Delta_2(\sigma)$ and Δ_{tr}, and the specific features observed in the PCs spectra of the MgB:LSMO composite due to magnetoelastic interaction (ph-mg) in LSMO (the curves are shifted for convenience).

pairing channels. In our case, it is reasonable to assume that relative weight of singlet and triplet components is determined by a ration of the composite's constituents. I.e., the *s*-wave component is due to a pairing in MgB_2 while the *p*-wave counterpart originated from an incoherent condensate in LSMO.

3.2. BW phase

Here we get in touch with a necessity to identify the *p*-wave state. This question will be discussed in details elsewhere. In short, our analysis has shown that in the case of a given composite, most probably, we deal with the so-called Balian–Werthamer (BW) state [21]. The BW superconducting state consists of an equal superposition of pairs with spin **S** ($|\mathbf{S}| = 1$) antiparallel to orbital momentum **L**. A pair total angular momentum, which is a true quantum number for a noncentrosymmetric superconductor, has no favored direction $\mathbf{J} = \mathbf{S} + \mathbf{L} = 0$. The gap function in the BW state has a constant product $\Delta\Delta^{\dagger} = \Delta_0^2$. In this phase the quasiparticles density of state (DOS) has the same form as that of the ordinary *s*-wave superconductor and the equilibrium thermodynamic properties of the BW state and the *s*-wave superconductor are identical [4].

To test our conclusion, a fitting of the total composite conductivity was done using different *p*-wave state symmetry. We used in our model calculations $Z = 0.1$ for the effec-

tive barrier parameter and $\Delta_{MgB} = 3.5$ meV for MgB_2 (this "average" value of a superconducting gap is typical for polycrystalline samples of MgB_2 [5]). The best adjustment was obtained if the energy gap of LSMO is equal to $\Delta_{tr} = 18$ meV for the BW phase. An example of such fitting is shown in Fig. 4. One can see that the case of the order parameter angular dependence as for the BW phase fits the experimental curve very well. To avoid confusion with the data shown in Fig. 4, note that both components j_{tr} and j_s exist at $eV < \Delta_{MgB}$, and only $j_{tr} \sim |\Psi_{tr}|^2$ part remains at $\Delta_{MgB} < eV < \Delta_{tr}$. By another words, supercurrent through a contact we can decomposed into two parts: fully unpolarized I_{un} and fully polarized I_{pol}. Fully polarized part exists at $|eV| < \Delta_{tr}$, while unpolarized only at $|eV| < \Delta_{MgB}$. That is why in the figure $G_S/G_N \approx 3$ at $eV < \Delta_{MgB}$. Note, in this connection, that a several-fold relative enhancement in the zero-bias conductance compared to its high-bias value is typically observed if a contact is made between a good normal metal and a superconductor with very large normal state resistivity [11]. For example, a fivefold enhancement is detected in a contacts made between an Y_2PdGe_3 polycrystalline superconductor and a Pt–Ir tip [11]. It is expected, that this enhancement arise from the critical current alone. Yet, a detailed satisfactory understanding of the origin of this several-fold relative enhancement in the zero-bias conductance is still lacking.

As already mentioned, due to the AR of quasiparticles at the N/S interface, the excess current appears in N-*c*-S contacts at $eV > \Delta$. Its magnitude is proportional to the superconducting energy gap [12]. In a general case, an observed magnitude of the excess current is $I_{exc} \approx q\Delta/eR_N$,

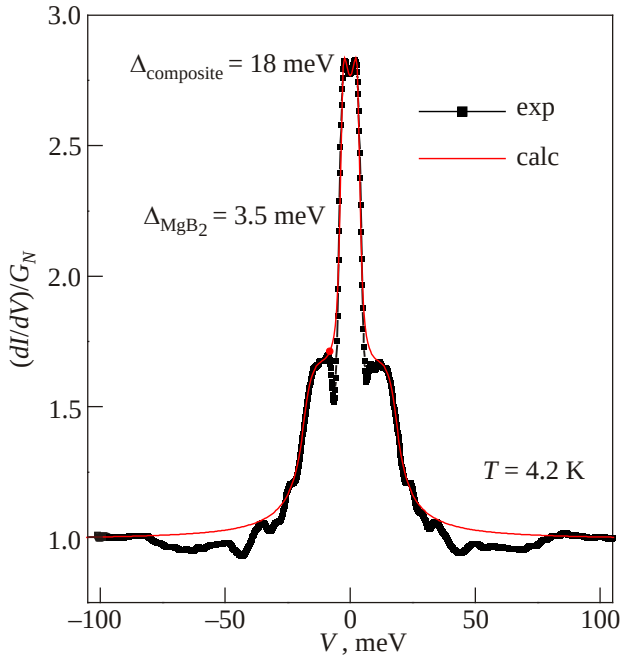

Fig. 4. (Color online) The PC experimental conductance and the fitting with the nodeless *p*-wave order parameter. (For the value of the parameters used, see the text.)

where the coefficient q depends on the symmetry of the order parameter and the quality of the constriction. Using this expression, it is easy to analyze the experimental data shown in Fig. 1. We choose in our model calculation that the pairing gap is equal to $\Delta_0 = 18$ meV. Then, for PC-1 with $I_{exc} \approx 12.6$ mA and $R_N \approx 1.58$ Ω we found $q \approx 1.1$; for PC-2 with $I_{exc} \approx 1.39$ mA and $R_N \approx 13.1$ Ω we obtained $q \approx 1.01$; and for PC-3 with $I_{exc} \approx 11.5$ mA and $R_N \approx 1.74$ Ω we received $q \approx 1.14$. On the other hand, using the expressions of Ref. 22, one can calculate I_{exc} for a hmF/*p*-wave S junction. For the BW phase we obtained: $I_{exc} = 1.22\Delta_0/eR_N$, with $\Delta_0 = 18$ meV, in reasonable agreement with the experimental results.

We also performed similar analysis for *p*-wave phases with other topology of order parameter; in particular, when the gap function has nodes on the Fermi surface. It was found that the order parameter with nodes could not fit the experimental results reasonably well. Thus, we think the *p*-wave superconducting state with nodeless order parameter is realized in the MgB:LSMO nanocomposite at $T < 30$ K.

3.3. Quasiparticles self-energy effects

The attractive features of PC spectroscopy is that the second derivatives of the *I–V* characteristic at large biases not only qualitatively but also semiquantitatively correspond to the self-energy effects in the superconducting order parameter [8]. These self-energy effects can be used in standard programs [23] to solve the Eliashberg equations [24] for quantitative derivation of electron–boson-interaction spectral function.

In the case of MgB:LSMO nanocomposite, it is obvious that the system contains several (no less than three) weakly connected charge carrier groups with quite different properties. Indeed, even for a separate MgB_2, one has to consider at least two types of charge carriers. One of those (σ-band) is two-dimensional with a strong EPI, while the other one (π-band) is three-dimensional with a weak EPI but with larger density of state at the Fermi energy. The inter-band scattering is weak and MgB_2 behaves as a *s*-wave superconductor with two distinct energy gaps (σ and π gaps) [5,6]. As for LSMO constituent, in the framework of the conventional double exchange model (see, e.g., [25]), there is complete splitting of majority and minority spin bands by large Hund's energy (~ 1 eV). At low temperature, spin of itinerant electrons of ferromagnetic manganites is completely polarized and the system is in a half-metallic state. Thus, if superconductivity can exist at all in this compound, it would most likely be of the *p*-wave triplet type with parallel spin pairs. Accordingly, a multiband model comprised of a superposition of pairs with a spin-triplet *p*-wave and spin-singlet *s*-wave components has to be applied in the case of MgB:LSMO system in a superconducting phase.

However, direct application of the Eliashberg equations in the case of a multiband superconductor is mathematically an ill-defined problem: it is not possible to obtain several band EPI functions $\alpha^2F_{ij}(\Omega)$ from a single $I(V)$ experimental dependence. (Here $\alpha = \alpha(\Omega)$ describes the strength of the electron interaction with a given phonon branch for electron transport through the contact and $F_{ij}(\Omega)$ stands for the phonon DOS.)

Since the nature of the pairing interaction in half-metallic manganite is unknown, we chose the following strategy to shed light on the question addressed. The phonon spectrum and the electron–phonon coupling in MgB_2 are well known at present (see Refs. 5, 16, 26–28). Using these data, we first calculate the *dI*/*dV*–*V* characteristics of a PC for the π- and σ-bands of MgB_2. Comparing (extracting) the contribution of the MgB_2 phonons with (from) the experimental *dI*/*dV*–*V* data for the composite, we will be able, at least in principle, to reveal the *dI*/*dV*–*V* nonlinearities which are due to a superconducting state of the LSMO constituent, if they are, and then to analyze them. With this in mind, let us calculate the contribution from MgB_2.

3.3.1. Contribution from the MgB_2 phonons. According to the conventional labeling [5], superconducting properties of MgB_2 can be described by an effective two (σ- and π-) bands model. Following the approach proposed by Brinkman *et al*. [27], the total current through a *tunnel* MgB_2–N structure is a sum of the components and, hence, the total normalized conductance can be written as a weighted sum of the contributions of the σ- and π-bands, where the weighting factors are determined by the plasma frequencies along the corresponding crystallographic directions. Thus, the normalized tunnel contact conductance is given by

$$G^{\gamma}(\omega) = A_{\gamma}^{\sigma} G_{\sigma}(\omega) + A_{\gamma}^{\pi} G_{\pi}(\omega), \quad \omega = eV \qquad (3)$$

with $\gamma = ab$ or c for a current flowing in the *ab* plane or in the *c* direction, respectively. Within the approximation of a δ-function barrier, the $G_{\sigma}(\omega)$ and $G_{\pi}(\omega)$ are the partial superconducting densities of states, respectively (for numerical values of the weighting parameters see Table 1 in Ref. 27). The contribution of the π-band is always dominant even if tunneling is almost in the *ab* plane.

Within the two-band model, for the conductance of a *metallic* MgB_2–N PC, one can obtain the expressions similar to Eqs. (3). However, now the partial conductance for σ- and π-bands, $G_{\sigma}(\omega)$ and $G_{\pi}(\omega)$ should be calculated within the framework of the generalized BTK model as discussed in Refs. 6, 27. The related normalized function can be expressed as Eq. (2), however, with a given band's label $\Delta_j(\varepsilon)$, $j = \pi$ or σ. The numerical values of the weighting parameters, strictly spiking, changed, too.

It is well known, in the Eliashberg approach, even in the weak-coupling regime a superconducting order parameter $\Delta(\omega)$ is a (complex) function of energy with an energy-dependent real and imaginary parts. Thus $\Delta_j(\omega) = \mathrm{Re}\,\Delta_j(\omega) + I\,\mathrm{Im}\,\Delta_j(\omega)$ for a current in c ($j = \pi$) or ab ($j = \sigma$) directions. We calculated the gap functions $\Delta_j(\omega)$ with an extension of the Eliashberg formalizm to a two bands superconductor (see, e.g., Ref. 27). These equations have been solved numerically using the EPI functions found recently in Refs. 27, 28 from the first principles calculations.

With the numerical data in hands for a MgB_2–N contact, we are able to reveal directly the self-effects due to the MgB_2 phonons in the experimental *dI*/*dV*–*V* data for the MgB:LSMO composite. As follows from the data (not shown here), at energies above the largest gap Δ_{tr} the contribution of the MgB_2 phonons into the total conductance of the MgB:LSMO PCs is *negligibly small*. In fact, one may expect this result because, as is seen from Eq. (2), at $\omega >> \Delta_{\sigma}$ the energy-dependent effects are of the order $(\Delta_{\sigma}/\omega)^2$. As far as the magnitude of the gap Δ_{tr} is about three times larger than Δ_{σ}, at $\omega >> \Delta_{tr}$ the contributions related to MgB_2 are weakened by an order.

3.3.2. Magnon–phonon self-energy effects. In diffusive S-*c*-N contacts the self-energy effects might appear already in the first derivative of their *I*–*V* characteristics (see, e.g., [15] and §12.1 in Ref. 8). Using the data obtained we attempt to identify the structure of the composite's PC spectra at energies typical for phonons and magnons. Yet, this is not so easy task.

The phonon spectra of ABO_3 perovskite structure usually are separated into "external", "bending" and "stretching" modes with respect to cubic ($Pm3m$) symmetry [29,30]. The "external" mode represents a vibrating motion of the A ion against the BO_3 octahedra, and two "internal" modes reflect internal motions of B and O ions in the octahedra ("bending" and "stretching" modes, respectively). Depending on the ion size and the doping concentration, these triply degenerate modes split into pairs of nondegenerate and doubly degenerate modes; moreover, they become broader and overlap [30–34]. Furthermore, due to large unit cell, additional modes emerge in the metallic phase of doped manganites. The phonon structures of the doped sample are broader and do not allow identifying strictly all the observed lines. Also the peak positions of phonons measured in a powder system can be shifted with respect to the real position in crystals [34,35].

In addition, there is much experimental and theoretical evidence in favor of the fundamental role of magnetoelastic coupling in physics of substituted manganite [25,36]. Strong magnon–phonon interaction is confirmed, in particular, by inelastic neutron scattering measurements, which point that magnetoelastic coupling is important for understanding of the low-temperature lattice and spin dynamics in ferromagnetic manganite. From the wave-vector dependence of the magnon lifetime and its association with the dispersions of selected optical phonon modes, it was argued that the observed magnon softening and broadening are due to strong magnon–phonon interactions [31–33].

In our case, the energy range where it is reasonable to expect "magnon traces" in *I–V* characteristic is at $eV \sim [\Delta_{tr}+\Delta_2(\sigma)]$ or at $eV \sim [\Delta_{tr}+\Delta_1(\pi)]$. Indeed, for the system under consideration, a crucial condition is the process of conversion of the spinless (spin-singlet) Cooper pair into spin-polarized (spin-triplet) Cooper pair and vice versa (some kind of an "intrinsic proximity" effect; for more detailed discussion see, e.g., reviews [37,38]). During this conversion, spin waves are emitted or absorbed.

Comparing typical PCs spectra nonlinearities (Figs. 2 and 3) with the phonon and magnon DOS restored in neutron measurements [29–33], we found a definite correlation between nonlinearities in the PCs spectra and these data. We think that specific peculiarities in the PC spectra at 20.9–30.2 meV, 38.2–38.6 meV, and 44.5–45.7 meV in Fig. 3 are due, most probably, to interaction of electrons with magnetoelastic waves. As for the electron–boson traces in PCs of composite with hmF LCMO, Fig. 2, here the number of distinctive peculiarities is significantly larger, and they are difficult to be identified strictly. Further detailed investigations are definitely needed to be sure that the distinctive features observed in the PCs spectra of the MgB:LSMO composite are due to electron–phonon or electron–magnon interactions in LSMO.

4. Summary

In this report, we addressed a pairing symmetry and a plausible pairing mechanism of a superconducting state that realizes in the MgB_2:$La_{0.65}Sr_{0.35}MnO_3$ nanocomposite. Taking into account that a superconducting phase develops in a low-symmetry environment with a missing inversion center, we considered a model of a ferromagnetic superconductor described by uniformly coexisting itinerant ferromagnetism and a mixed-parity superconducting state. In this state the order parameter, most probably, possesses a nodeless topology and the single-electron DOS has the same form as that of the ordinary *s*-wave superconductor. Utilizing the extended Eliashberg formalizm, we calculated the contribution of MgB_2 in the total composite conductivity and estimated a magnitude of the electron–phonon singularities originated from the MgB_2 in the *I–V* characteristics of the composite. It was found that distinctive features observed in the PC spectra of the MgB:LSMO composite can not be related to the phonons of MgB_2. The singularities observed in the *I–V* characteristics at above-gap energies may be a manifestation of the electron spectrum renormalizations due to strong magnon–phonon (magnetoelastic) interaction in $La_{0.65}Sr_{0.35}MnO_3$. Yet, the conventional point-contact spectroscopy investigations of the second derivatives of the PC's *I–V* characteristics at large biases are definitely needed to identify the electron–phonon (electron–magnon) self-energy structure in a superconducting state of the nanocomposite. The results propose a new route to unconventional superconductivity and, we hope, can motivate the search for new material for superconducting spintronics.

The authors thanks to M. Belogolovskii, A. Omelyanchouk, and Yu. Naidyuk for useful discussions.

1. V.N. Krivoruchko and V.Yu. Tarenkov, *Phys. Rev. B* **86**, 10502 (2012).
2. V.N. Krivoruchko and V.Yu. Tarenkov, *Phys. Rev. B* **75**, 214508 (2007).
3. V.N. Krivoruchko and V.Yu. Tarenkov, *Phys. Rev. B* **78**, 054522 (2008).
4. V.P. Mineev and K.V. Samokhin, *Introduction to Unconventional Superconductivity*, Gordon and Breach, New York (1999).
5. X.X. Xi, *Rep. Prog. Phys.* **71**, 116501 (2008).
6. D. Daghero and R.S. Gonnelli, *Supercond. Sci. Technol.* **23**, 043001 (2010).
7. D. Fay and J. Appel, *Phys. Rev. B* **22**, 3173 (1980).
8. Y.G. Naidyuk and I.K. Yanson, *Point-Contact Spectroscopy*, Springer Series in Solid State Science, v. **145**, New York: Springer (2005).
9. M.M. Savosta, V.N. Krivoruchko, I.A. Danilenko, V.Yu. Tarenkov, T.E. Konstantinova, A.V. Borodin, and V.N. Varyukhin, *Phys. Rev. B* **69**, 024413 (2004).
10. A.S. Mazur, V.N. Krivoruchko, and I.A. Danilenko, *Fiz. Nizk. Temp.* **33**, 1222 (2007) [*Low Temp. Phys.* **33**, 931 (2007)].
11. G. Sheet, S. Mukhopadhyay, and P. Raychaudhuri, *Phys. Rev. B* **69**, 134507 (2004).
12. A.V. Zaitsev, *Zh. Eksp. Teor. Fiz.* **78**, 221 (1980).
13. V.A. Khlus and A.N. Omelyanchuk, *Fiz. Nizk. Temp.* **9**, 373 (1983) [*Sov. J. Low Temp. Phys.* **9**, 189 (1983)].
14. V.A. Khlus, *Fiz. Nizk. Temp.* **9**, 985 (1983) [*Sov. J. Low Temp. Phys.* **9**, 510 (1983)].
15. A.N. Omelyanchuk, S.I. Beloborod'ko, and I.O. Kulik, *Fiz. Nizk. Temp.* **14**, 1142 (1988) [*Sov. J. Low Temp. Phys.* **14**, 630 (1988)].
16. I.K. Yanson, S.I. Beloborod'ko, Yu.G. Naidyuk, O.V. Dolgov, and A.A. Golubov, *Phys. Rev. B* **69**, 100501(R) (2004).
17. A.F. Andreev, *Sov. Phys. JETP* **19**, 1228 (1964).
18. G.J. Strijkers, Y. Ji, F.Y. Yang, C.L. Chien, and J.M. Byers, *Phys. Rev. B* **63**, 104510 (2001).
19. R.C. Dynes, V. Narayanamuri, and J.P. Garno, *Phys. Rev. Lett.* **41**, 1509 (1978).
20. L. Gor'kov and E. Rashba, *Phys. Rev. Lett.* **87**, 037004 (2001).
21. R. Balian and N.R. Werthamer, *Phys. Rev.* **131**, 1553 (1963).
22. S. Kashiwaya, Y. Tanaka, M. Koyanagi, and K. Kajimura, *Phys. Rev. B* **53**, 2667 (1996).
23. A.I. D'yachenko, *cond-mat/0309479* (2003).
24. E.L. Wolf, *Principles of Electron Tunneling Spectroscopy*, Oxford University Press, London (1985).
25. E. Dagotto, T. Hotta, and A. Moreo, *Phys. Rep.* **344**, 1 (2001).
26. I.K. Yanson, V.V. Fisun, N.L. Bobrov, Yu.G. Naidyuk, W.N. Kang, Eun-Mi Choi, Hyun-Jung Kim, and Sung-Ik Lee, *Phys. Rev. B* **67**, 024517 (2003).

27. A. Brinkman, A.A. Golubov, H. Rogalla, O.V. Dolgov, J. Kortus, Y. Kong, O. Jepsen, and O. K. Andersen, *Phys. Rev. B* **65**, 180517(R) (2002).
28. O. De la Peña-Seaman, R. de Coss, R. Heid, and K.-P. Bohnen, *Phys. Rev. B* **82**, 224508 (2010).
29. A.V. Boris, N.N. Kovaleva, A.V. Bazhenov, P.J.M. van Bentum, Th. Rasing, S.-W. Cheong, A.V. Samoilov, and N.-C. Yeh, *Phys. Rev. B* **59**, R697 (1999).
30. A. Paolone, P. Roy, A. Pimenov, A. Loidl, O.K. Melnikov, and A.Y. Shapiro, *Phys. Rev. B* **61**, 11255 (2000).
31. M. Hennion, F. Moussa, P. Lehouelleur, F. Wang, A. Ivanov, Y.M. Mukovskii, and D. Shulyatev, *Phys. Rev. Lett.* **94**, 057006 (2005).
32. P. Dai, H.Y. Hwang, J. Zhang, J.A. Fernandez-Baca, S.-W. Cheong, C. Kloc, Y. Tomoika, and Y. Tokura, *Phys. Rev. B* **61**, 9553 (2000).
33. S. Petit, M. Hennion, F. Moussa, D. Lamago, A. Ivanov, Y.M. Mukovskii, and D. Shulyatev, *Phys. Rev. Lett.* **102**, 207201 (2009).
34. K.H. Kim, J.Y. Gu, H.S. Choi, G.W. Park, and T.W. Noh, *Phys. Rev. Lett.* **77**, 1877 (1996).
35. I. Fedorov, J. Lorenzana, P. Dore, G. De Marzi, P. Maselli, P. Calvani, S.-W. Cheong, S. Koval, and R. Migoni, *Phys. Rev. B* **60**, 11875 (1999).
36. J. Zhang, F. Ye, H. Sha, P. Dai, J.A. Fernandez-Baca, and E.W. Plummer, *J. Phys.: Condens. Matter* **19**, 315204 (2007).
37. M. Eschrig, T. Löfwander, T. Champel, J.C. Cuevas, J. Kopu, and G. Schön, *J. Low Temp. Phys.* **147**, 457 (2007).
38. V.N. Krivoruchko, A.I. D'yachenko, and V.Yu. Tarenkov, *Fiz. Nizk. Temp.* **39**, 276 (2013) [*Low Temp. Phys.* **39**, 211 (2013)].